Discotic liquid crystals of transition metal complexes 52†: Synthesis and homeotropic alignment of liquid crystalline phthalocyanine-fullerene dyad bridged by vanillin

Ayumi Watarai [a], Kazuchika Ohta*[a] and Mikio Yasutake[b]

[a]*Smart Material Science and Technology, Interdisciplinary Graduate School of Science and Technology, Shinshu University, 1-15-1 Tokida, Ueda, 386-8567, Japan.*

[b]*Comprehensive Analysis Centre for Science, Saitama University, 255 Shimo-okubo, Sakura-ku, Saitama 338-8570, Japan.*

Received date (to be automatically inserted after your manuscript is submitted)
Accepted date (to be automatically inserted after your manuscript is accepted)

ABSTRACT: We have synthesized a novel liquid crystalline phthalocyanine(Pc)-fullerene(C_{60}) dyad **$(C_{14}S)_6$PcCu-VAN-C_{60}** (**3a**) bridged by an inexpensive natural product of vanillin (**VAN**), instead of the previous long *n*-alkylene chain spacer. We have also synthesized a comparative dyad **$(C_{14}S)_6$PcCu-OPh-C_{60}** (**3b**) bridged by *p*-hydroxybenzaldehyde (**OPh**), in order to investigate the influence of the methoxy group in the vanillin moiety on homeotropic alignment between two glass plates. Very interestingly, homeotropic alignment could be observed only for the dyad **$(C_{14}S)_6$PcCu-VAN-C_{60}** (**3a**) having a methoxy group in the vanillin moiety, whereas it could not be observed for the dyad **$(C_{14}S)_6$PcCu-OPh-C_{60}** (**3b**) having no methoxy group at the phenoxy group. It is very noteworthy that such a slight difference in these molecular structures between **3a** and **3b** becomes a crucial point to show the homeotropic alignment. Each of the dyads, **3a** and **3b**, showed two hexagonal ordered columnar (Col_{ho}) mesophases. Each of the Col_{ho} mesophases in **3a** and **3b** gave an additional very strong reflection peak named as Peak H in a very low angle region of the SAXS (small angle X-ray scattering) pattern. Peak H could be established, from two different SAXS measurement methods, as one pitch in a helical structure of the fullerenes around the Pc column.

KEYWORDS: Phthalocyanine, fullerene, vanillin, columnar mesophase, homeotropic alignment, helical structure

*Correspondence to: Smart Material Science and Technology, Interdisciplinary Graduate School of Science and Technology, Shinshu University, 1-15-1 Tokida, Ueda, 386-8567, Japan. E-mail: ko52517@shinshu-u.ac.jp; Fax: +81-268-21-5492; Tel: +81-268-21-5492

†Part 51: Yoshioka M, Ohta K, Miwa Y, Kutsumizu S, Yasutake M. *J. Porphyrins Phthalocyanines*, 2014; **18**: 856–868.

INTRODUCTION

Recently, organic thin-film solar cells have been very much attention as the next generation solar cells to replace the present silicon solar cells. Although the energy conversion efficiency of silicon solar cells is high enough, the production cost and energy are still high. On the other hand, organic thin-film solar cells are so flexible and lightweight that we may reduce the production cost by the film formation in large area with easy device processing techniques [1-3]. It is very advantageous for the practical mass production. However, the conversion efficiency of organic thin-film solar cells is lower than that of silicon solar cells. Therefore, the research works are world-widely carried out in order to improve the conversion efficiency of organic thin-film solar cells.

It is important for organic thin-film solar cells to form efficient charge separation. When the donor molecules absorb sunlight, the excitons are formed and move to the interface between donors and acceptors. At the interface, the excitons separate into electrons and holes, which flow in the opposite directions thorough the acceptor and donor layers, respectively. Bulk hetero junction structure, in which the domains of electron-donor and electron-acceptor are randomly arranged, has been generally employed. The interface area of bulk hetero junction is larger than conventional two-layered hetero junction. However, it is very difficult to control the interface structure and molecular arrangement of donors and acceptors in the bulk hetero junction. In 2009, Yoshikawa *et al*. proposed a novel one-dimensional nano array structure of donors and acceptors. By using this 1D nano array structure we can expect both the interface area increase and ideal molecular arrangement to improve the conversion efficiency [4].

Recently, columnar liquid crystalline donor acceptor (D-A) dyads consisting of both donor and acceptor parts in a molecule have been actively investigated [5-32], because they can be applied to flexible organic thin film solar cells. As far as we know, the first liquid crystals based on phthalocyanine fullerene (Pc-C_{60}) dyad (Fig. 1[A]) were reported by our group in 2006 [10-22] and then Geerts group in 2009 [14]. Among our liquid crystalline Pc-C_{60} dyads, we found at the first time in 2006 that some of the Pc-C_{60} dyads exhibit perfect homeotropic alignment between two glass plates (Fig. 1[B]) [10-22, 15-18, 20-23, 27-32]. It is very interesting that the perfect homeotropic alignment of the liquid crystalline Pc-C_{60} dyad is compatible with the 1D nano array structure proposed by Yoshikawa *et al*. [4]. In 2009, we found at the first time an additional large peak in a very low angle region of their SAXS (small angle X-ray scattering) patterns of the columnar mesophases [15-18, 20-22]. The additional peak could not be assigned as a reflection from any two-dimensional lattices of columnar liquid crystals known up to date, so that we assigned this peak as a helical pitch of C_{60} moieties around the Pc column, and we described a schematic model of the C_{60} helical structure around the Pc column [15-18, 20-22], as illustrated in Fig. 1[C]. To more establish the helical structure of C_{60} moieties, we adopted a new monodomain method (like as single crystal method) [23, 30-32] together with the conventional polydomain method (like as powder crystal method) [15-18, 20-32] for the SAXS measurements. From these two different methods, we could thoroughly establish this additional peak as a helical pitch in Z-axis direction, at the first time in 2011 [23, 30-32]. The helical structure very resembles spiranthes flowers, so that we named this unique structure as "spiranthes-like supramolecular structure" [31, 32]. On the other hand, in 2010-11 Imahori and Shimizu joint research group also reported the helical structure of C_{60} moieties in a Pc-C_{60} dyad [19, 24, 25].

We are very interested in a relationship between the molecular structure of liquid crystalline Pc-C_{60} derivatives and appearance of the homeotropic alignment. In our recent works, we have successfully synthesized novel dyads, **$(C_nS)_6$PcCu-C_m-C_{60} (2a-g)** (Fig. 2[A]), exhibiting perfect homeotropic alignment [31, 32]. The donor part of hexakisalkylthio-substituted PcCu, **$(C_nS)_6$PcCu-**, could be synthesized in much shorter synthetic route than that of the previous hexakis(di-*m*, *p*-dialkoxyphenoxy)-substituted PcCu part, **[$(C_nO)_2$PhO]$_6$PcCu-,** (Fig. 1[C]). Furthermore, the

$(C_nS)_6$PcCu-C_m-C_{60} dyads (**2a-c**) exhibit homeotropic alignment at rt for (n, m) = (14, 8), (14, 10), (14, 12). Hence, the donor part of hexakistetradecylthio-substituted PcCu, **$(C_{14}S)_6$PcCu-**, may be favourable to induce a room temperature liquid crystalline phase. If the spacer part between Pc and C_{60} can be furthermore replaced by an inexpensive natural product of vanillin, a novel Pc-C_{60} dyad, **$(C_{14}S)_6$PcCu-VAN-C_{60}** (A = OCH_3: **3a** in Fig. 2[B]), can be more easily prepared in comparison with the previous dyads, **$(C_nS)_6$PcCu-C_m-C_{60}** (Fig. 2[A]). Therefore, we have synthesized, in this work, the novel liquid crystalline Pc-C_{60} dyad, **$(C_{14}S)_6$PcCu-VAN-C_{60}** (**3a**) together with a comparative dyad, **$(C_{14}S)_6$PcCu-OPh-C_{60}** (A = H: **3b** in Fig. 2[B]), in order to investigate the influence of the methoxy group on their homeotropic alignment. As a result, the homeotropic alignment could be observed only in the hexagonal ordered columnar (Col_{ho}) mesophases of the dyad **$(C_{14}S)_6$PcCu-VAN-C_{60}** (**3a**) having a methoxy group in the vanillin moiety, whereas it could not be observed in the Col_{ho} mesophases of the dyad **$(C_{14}S)_6$PcCu-OPh-C_{60}** (**3b**) having no methoxy group at the phenoxy group. Moreover, an additional very strong reflection peak appeared in a very low angle region of the SAXS pattern for each of the Col_{ho} mesophases in **3a** and **3b** could be established, also from two different SAXS measurement methods mentioned above, as one pitch in a helical structure of the fullerenes around the Pc column.

We wish to report here the interesting mesomorphism of these novel Pc-C_{60} dyads **3a** and **3b**.

EXPERIMENTAL

Synthesis

The Pc-C_{60} derivatives (**3a-b**) were synthesized according to Scheme 1. The phthalonitrile (**5**) was prepared by the method of Wöhrle *et al.* [33]. The phthalonitriles (**7a-b**) were prepared by the method of Serin *et al.* [34] by using 4-nitrophthalonitrile, vanillin and/or *p*-hydroxybenzaldehyde purchased from Tokyo Kasei. The Pc precursors, **($(C_{14}S)_6$PcCu-VAN-CHO** (**4a**) and **$C_{14}S)_6$PcCu-OPh-CHO** (**4b**), were synthesized by cyclic tetramerization reaction of these two types of phthalonitrile derivatives (**5** and **7a-b**). Finally, the target compounds, **$(C_{14}S)_6$PcCu-VAN-C_{60}** (**3a**) and **$(C_{14}S)_6$PcCu-OPh-C_{60}** (**3b**), were synthesized from **4a-b** with N-methyglycine and fullerene by Prato reaction [35]. We have described the details of these syntheses below. The compounds were characterized using ^{1}H-NMR, FT-IR, elemental analysis (Table S1), MALDI-TOF mass spectra (Table S1) and UV-vis spectra (Table S3).

4,5-Bis(tetradecylthio)phthalonitrile (5)

A mixture of 4,5-dichlorophthalonitrile (0.750 g, 3.81 mmol), tetradecane-1-thiol (2.11 g, 9.14 mmol), dry DMSO (7 ml) and potassium carbonate (2.21 g, 15.2 mmol) was heated at 110 ^oC for 2h with stirring under nitrogen atmosphere. After cooling to rt, the reaction mixture was extracted with chloroform and washed with brine. The organic layer was dried over Na_2SO_4 and evaporated in *vacuo*. The residue was purified by column chromatography (silica gel, chloroform, Rf = 0.78), and then by recrystallization from *n*-hexane to afford 1.39 g of white powder (Yield: 62.2%, mp: 64.7 ^oC (lit. 65.3 ^oC [32])).

IR (KBr, cm^{-1}): 2919.61, 2850.14 (-CH_2-), 2227.32 (-CN), 1562.96 (C=C).

^{1}H-NMR ($CDCl_3$, TMS [ppm]): δ = 7.40 (s, 2H, Ar-H), 3.01 (t, 4H, J = 8.6 Hz, -S-CH_2-), 1.79~1.70 (m, 4H, -CH_2-), 1.26 (m, 44H, -CH_2-), 0.88 (s, 6H, -CH_3).

4-(4-Formyl-1-methoxyphenoxy)phthalonitrile (7a)

A mixture of 4-nitrophthalonitrile (0.312 g, 1.80 mmol), vanillin (**6a**: 0.302 g, 1.98 mmol), dry DMSO (6 ml) and potassium carbonate (1.07 g, 7.71 mmol) was stirred under nitrogen atmosphere at rt for 29h. Since the raw material still remained, vanillin (**6b**: 0.123 g, 0.808 mmol) and potassium carbonate (0.252 g, 1.82 mmol) were added and the mixture was stirred under nitrogen atmosphere at rt for 43 more hours. The reaction mixture was extracted with dichloromethane and washed with brine. The organic layer was dried over Na_2SO_4 and evaporated in *vacuo*. The

residue was purified by recrystallization from methanol. After removal of the solvent, pale yellow powder was obtained (0.295 g, Yield: 59.0%, mp: 183.7 ^{o}C).

IR (CsI cm^{-1}): 2911.88 (-CH_3), 2853.18 (-CHO), 2232.40 (-CN).

^{1}H-NMR (DMSO-d_6, TMS [ppm]): δ = 10.0 (s, 1H, -C*H*O), 8.07~8.09 (d, J = 8.9 Hz, 1H, CN-Ar-*H*) , 7.78~7.79 (d, J = 2.5 Hz, 1H, Ar-*H*) , 7.71 (d, J = 2.2 Hz, 1H, CN-Ar-*H*), 7.65~7.67 (dd, J_1 = 8.9 Hz, J_2 = 2.4 Hz, 1H, CN-Ar-*H*) , 7.44~7.46 (d, J = 8.5 Hz, 1H, Ar-*H*) , 7.35~7.37 (dd, J_1 = 8.1 Hz, J_2 = 2.0 Hz, 1H, Ar-*H*), 3.83 (s, 3H, -O*CH*$_3$).

4-(4-Formylphenoxy)phthalonitrile (7b)

A mixture of 4-nitrophthalonitrile (1.00 g, 5.78 mmol), dry DMSO (15 ml), *p*-hydroxybenzaldehyde (**6b**: 0.775 g, 6.35 mmol) and potassium carbonate (1.07 g, 7.71 mmol) was stirred under nitrogen atmosphere at rt for 28h. The reaction mixture was extracted with dichloromethane and washed with brine. The organic layer was dried over Na_2SO_4 and evaporated in *vacuo*. The residue was purified by column chromatography (silica gel, dichloromethane, Rf = 0.39). After removal of the solvent, white powder was obtained (0.936 g, Yield: 65.2%, mp: 146.1 ^{o}C).

IR (KBr, cm^{-1}): 3105.49, 3072.56 (Ar-H), 2918.90, 2853.05 (-CHO), 2232.93 (-CN), 1689.63 (C=O).

^{1}H NMR (DMSO-d_6, TMS [ppm]): δ = 10.0 (s, 1H, -C*H*O), 8.18 (d, J = 8.6 Hz, 1H, CN-Ar-*H*), 8.05-8.00 (m, 2H, Ar-*H*), 7.98 (d, J = 2.5 Hz, 1H, CN-Ar-*H*), 7.59 (dd, J_1 = 8.8 Hz, J_2 = 2.5 Hz, 1H, CN-Ar-*H*), 7.39-7.35 (m, 2H, Ar-*H*).

($C_{14}S)_6$PcCu-VAN-CHO (4a)

A mixture of 4,5-bis(tetradecylthio)phthalonitrile (**5**: 0.500 g, 0.855 mmol), 4-(4-formylphenoxy)phthalonitrile (**7a**: 0.0803 g, 0.289 mmol), $CuCl_2$ (0.0764 g, 0.569 mmol), 1-hexanol (14ml) and DBU (3 drops) was refluxed under nitrogen atmosphere for 7h. After cooling to rt, methanol was poured into the reaction mixture to precipitate the target compound. The methanolic layer was removed by filtration. The residue was washed with methanol, ethanol and acetone successively. The residue was purified by column chromatography (silica gel, chloroform, Rf = 0.88), and then by column chromatography (silica gel, chloroform : n-hexane = 7 : 3, Rf = 0.70). After removal of the solvent, dark green liquid crystal was obtained (0.0541 g, Yield: 8.9%).

Elemental analysis: See Table S1.

MALDI-TOF mass spectral data: See Table S2.

UV-vis spectral data: See Fig. 3 and Table S3.

Phase transition temperatures: See Table 1.

($C_{14}S)_6$PcCu-OPh-CHO (4b)

A mixture of 4,5-bis(tetradecylthio)phthalonitrile (**5**: 0.608 g, 1.03 mmol), 4-(4-formylphenoxy)phthalonitrile (**7b**: 0.0858 g, 0.342 mmol), $CuCl_2$ (0.0923 g, 0.684 mmol), 1-hexanol (12ml) and DBU (3 drops) was refluxed under nitrogen atmosphere for 7h. After cooling to rt, methanol was poured into the reaction mixture to precipitate the target compound. The methanolic layer was removed by filtration. The residue was washed with methanol, ethanol and acetone successively. The residue was purified by column chromatography (silica gel, chloroform, Rf = 0.91), and then by column chromatography (silica gel, chloroform: n-hexane = 3 : 2, Rf = 0.48). After removal of the solvent, dark green liquid crystal was obtained (0.0584 g, Yield: 8.2%).

Elemental analysis: See Table S1.

MALDI-TOF mass spectral data: See Table S2.

UV-vis spectral data: See Fig. 3 and Table S3.

Phase transition temperatures: See Table 1.

($C_{14}S)_6$PcCu-VAN-C_{60} (3a)

A mixture of **($C_{14}S)_6$PcCu-VAN-CHO** (**4a**: 0.0301 g, 0.0144 mmol), fullerene (0.0214 g, 0.0270 mmol), N-methylglycine (0.0040 g, 0.0449 mmol) and dry toluene (6ml) was refluxed under nitrogen atmosphere for 28h. After

cooling to rt, the reaction mixture was extracted with chloroform and washed with brine. The organic layer was dried over Na_2SO_4 and evaporated in *vacuo*. The residue was resolved in a small amount of mixture solvent (chloroform : *n*-hexane = 1 : 9 v/v), and it was put into a very short column(diameter: 4.0 cm; length: 8.0 cm; alumina gel). The unreacted fullerene was removed by using *n*-hexane as the first eluent and then the target **$(C_{14}S)_6$PcCu-VAN-C_{60}** (**3a**) was collected by using chloroform as the second eluent. Then, further purification was carried out by using HPLC(toluene). After removal of the solvent, dark green liquid crystal was obtained (0.0117 g, Yield: 28.6%).

MALDI-TOF mass spectral data: See Table S2.

UV-vis spectral data: See Fig. 3 and Table S3.

Phase transition temperatures: See Table 1.

$(C_{14}S)_6$PcCu-OPh-C_{60} (3b)

A mixture of $(C_{14}S)_6$PcCu-VAN-CHO (**4b**: 0.0509 g, 0.0242 mmol), fullerene (0.0367 g, 0.0509 mmol), N-methylglycine (0.0046 g, 0.0581 mmol) and dry toluene (10ml) was refluxed under nitrogen atmosphere for 30h. After cooling to rt, the reaction mixture was extracted with chloroform and washed with brine. The organic layer was dried over Na_2SO_4 and evaporated in *vacuo*. The residue was resolved in a small amount of mixture solvent (chloroform : *n*-hexane = 1 : 9 v/v), and it was put into a very short column(diameter: 4.0 cm; length: 8.0 cm; alumina gel). The unreacted fullerene was removed by using *n*-hexane as the first eluent and then the target **$(C_{14}S)_6$PcCu-OPh-C_{60}** (**3b**) was collected by using chloroform as the second eluent. It was further purified by column chromatography (silica gel, chloroform : n-hexane = 7 : 3 v/v, Rf = 0.94). Then, it was purified by using HPLC (toluene). After removal of the solvent and dryness, dark green liquid crystal was obtained (0.0105 g, Yield: 15.4%).

MALDI-TOF mass spectral data: See Table S2.

UV-vis spectral data: See Fig. 3 and Table S3.

Phase transition temperatures: See Table 1.

Measurements

HPLC was carried out by using an LC-9110 NEXT of Japan Analytical Industry Co. Ltd. The infrared absorption spectra were recorded by using a Nicolet NEXUS670 FT-IR. The ^{1}H-NMR measurements were carried out by using a Bruker Ultrashield 400 MHz. The elemental analyses were performed by using a Perkin-Elmer Elemental Analyzer 2400. The MALDI-TOF mass spectral measurements were carried out by using a Bruker Daltonics Autoflex III spectrometer (matrix: dithranol). Electronic absorption (UV-vis) spectra were recorded by using a Hitachi U-4100 spectrophotometer. Phase transition behaviour of the present compounds was observed with polarizing optical microscope (Nikon ECLIPSE E600 POL) equipped with a Mettler FP82HT hot stage and a Mettler FP90 Central Processor, and a Shimadzu DSC-50 differential scanning calorimeter. The mesophases were identified by using a small angle X-ray diffractometer (Bruker Mac SAXS System) equipped with a temperature-variable sample holder adopted a Mettler FP82HT hot stage. Figs. S1 and S2 illustrate the setup of the SAXS system and the setup of the temperature-variable sample holder, respectively. As can be seen from Fig. S1, the generated X-ray is bent by two convergence monochrometers to produce point X-ray beam (diameter = 1.0 mm). The point beam runs through holes of the temperature-variable sample holder. As illustrated in Fig. S2, into the temperature-variable sample holder of Mettler FP82HT hot stage, a glass plate (76 mm × 19 mm × 1.0 mm) having a hole (diameter = 1.5 mm) is inserted. The hole can be charged with a powder sample (*ca.* 1 mg). The measurable range is from 3.0 Å to 110 Å and the temperature range is from rt to 375 °C. This SAXS system is available for all condensed phases including fluid nematic phase and isotropic liquid.

RESULTS AND DISCUSSION

Phase transition behaviour

Table 4 lists up phase transition temperatures and enthalpy changes of **$(C_{14}S)_6$PcCu-VAN-CHO** (**4a**), **$(C_{14}S)_6$PcCu-OPh-CHO** (**4b**), **$(C_{14}S)_6$PcCu-VAN-C_{60}** (**3a**) and **$(C_{14}S)_6$PcCu-OPh-C_{60}** (**3b**). These phase transition behaviours were characterized using differential scanning calorimeter (DSC), polarizing optical microscope (POM) and temperature-dependent small angle X-ray diffraction measurements.

As can be seen from this table, each of the Pc precursors, **$(C_{14}S)_6$PcCu-VAN-CHO** (**4a**) and **$(C_{14}S)_6$PcCu-OPh-CHO** (**4b**), showed only one hexagonal ordered columnar (Col_{ho}) mesophase from rt. On heating from rt, the Col_{ho} mesophases did not show any mesophase-mesophase transition until high temperatures, and directly cleared into isotropic liquid (I.L.) with gradual decomposition (dc). When the I.L. was quickly cooled down below the clearing point with avoiding the decomposition, a dendric texture characteristic to a hexagonal columnar (Col_h) phase was appeared, as shown in Fig. 4[A] and [B].

As can be seen from Table 1, the **$(C_{14}S)_6$PcCu-VAN-C_{60}** (**3a**) dyad having a methoxy at the phenoxy group showed two different hexagonal columnar mesophases, Col_{ho1} and Col_{ho2}. When the Col_{ho1} mesophase was heated from rt, it transformed in to the Col_{ho2} mesophase at 83.5 ^oC; on further heating, the Col_{ho2} mesophase cleared into I.L. at 178.3 ^oC. When the I.L. was cooled down to 120 ^oC in the Col_{ho1} mesophase temperature region and then to rt in the Col_{ho2} mesophase temperature region, both the Col_{ho1} and Col_{ho2} mesophases showed completely darkness without birefringence under crossed Nicols, as can be seen from photomicrographs in Fig. 5[A]. This suggested that perfect homeotropic alignment was formed both the Col_{ho1} and Col_{ho2} mesophases. When the film in the dark field was scratched with a spatula, the scratched part became birefringent. In the bottom of Fig. 5[A] are illustrated the hoemotropic alignment models. When disk-like molecules face-to-face stack one after another to form columns perpendicular to the glass substrate, homeotropic alignment is achieved to show the dark field under crossed Nicols. When the columns perpendicular to the glass substrate is disturbed by scratching with a spatula, the disturbed area may become birefringent. Thus, we could certify the homeotropic alignment of the **$(C_{14}S)_6$PcCu-VAN-C_{60}** (**3a**) dyad, as can be seen from the photomicrographs in Fig. 5[A].

As can be seen also from Table 1, the **$(C_{14}S)_6$PcCu-OPh-C_{60}** (**3b**) dyad having no methoxy group at the phenoxy group also showed two different hexagonal columnar mesophases, Col_{ho1} and Col_{ho2}. When the Col_{ho1} mesophase was heated from rt, it transformed into to Col_{ho2} mesophase at 96.5 ^oC. On further heating, the Col_{ho2} mesophase cleared into I.L. at 176.7 ^oC. When the I.L. was cooled down to 120 ^oC, a sanded texture appeared for the Col_{ho2} mesophase, as can be seen from Fig. 5[B]; on further cooling into the Col_{ho1} mesophase temperature region, the Col_{ho1} mesophase also gave birefringence, as can be seen from Fig. 5[B]. Thus, the dyad **3b** does not show homeotropic alignment.

It is very noteworthy that the dyad **$(C_{14}S)_6$PcCu-VAN-C_{60}** (**3b**) having a methoxy at the phenoxy group shows homeotropic alignment, whereas the dyad **$(C_{14}S)_6$PcCu-OPh-C_{60}** (**3a**) having no methoxy group at the phenoxy group does not show homeotropic alignment.

Temperature-dependent X-ray diffraction study

In Table 2 are summarized the X-ray data of the Pc precursors, **$(C_{14}S)_6$PcCu-VAN-CHO** (**4a**) and **$(C_{14}S)_6$PcCu-OPh-CHO** (**4b**), and the corresponding Pc-C_{60} dyads, **$(C_{14}S)_6$PcCu-VAN-C_{60}** (**3a**) and **$(C_{14}S)_6$PcCu-OPh-C_{60}** (**3b**). As can be seen from this table, each of the mesophases in **3a**, **3b**, **4a** and **4b** could be identified from the X-ray diffraction study as a hexagonal ordered columnar (Col_{ho}) mesophase.

Helical structure of fullerene moieties in 3a and 3b established by SAXS

Very interestingly, these Col_{ho} mesophases in **3a** and **3b** gave an additional large peak in a very low angle region of $2\theta \approx 1.5^{o}$ (*ca*. 60 Å) of their SAXS (small angle X-ray scattering) patterns. We named this additional peak as Peak H which we found also in our previous PcCu-C_{60} dyads at the first time in 2009 [15-18, 20-22]. This peak H could not be assigned to a reflection from any two-dimensional lattices in columnar mesophases known up to date, so that we assigned this peak as a helical pitch of C_{60} moieties around the Pc column, and we described a schematic model of the C_{60} helical structure around the Pc column [15-18, 20-22], as illustrated in Fig. 1[C]. At the first time in 2011, we adopted a new monodomain method, together with the conventional polydomain method [15-18, 20-22], illustrated in Fig. 6[A] and [B], respectively, and thoroughly established this peak H as a helical pitch in Z-axis direction [23, 30-32] from these two different methods. Also by using these methods, we could establish here the helical structure of C_{60} moieties around the Pc columns for the present dyad **$(C_{14}S)_6$PcCu-VAN-C_{60}** (**3a**).

Fig. 6 also illustrates the X-ray diffraction patterns of **$(C_{14}S)_6$PcCu-VAN-C_{60}** (**3a**) by using these two methods [A] and [B]. The red X-ray diffraction pattern in this figure was measured by Polydomain Method [A]. As can be seen from this red pattern, both Peak H and (1 0 0) reflection could be clearly observed. The black and blue X-ray diffraction patterns in this figure were measured by Method [B]. The black diffraction pattern was measured for only two cover glass plates without the sample. It gave no peak. The blue X-ray diffraction pattern was measured for the **$(C_{14}S)_6$PcCu-VAN-C_{60}** (**3a**) dyad sandwiched between two cover glass plates. As can be seen from this blue diffraction pattern, it gave (1 0 0) reflection but Peak H disappeared. This means that Peak H is the periodicity in Z-direction.

Moreover, Peak H did not appear in the Col_{ho} mesophases of **4a** and **4b**, but appeared only in the Col_{ho} mesophases of **3a** and **3b**. Therefore, Peak H could be attributed to the fullerene moieties. Unless the fullerenes would be helically staked in the Z-direction, the fullerene balls having diameter = 10 Å could not pile up around the column having the stacking distance between the flat Pc disks = *ca*. 3.5 Å. Hence, Peak H could be assigned to one pitch in a helical structure of the fullerenes.

Peak H height difference

Fig. 7[A] shows X-ray diffraction patterns of the Col_{ho} mesophases at rt for the present dyads, **$(C_{14}S)_6$PcCu-VAN-C_{60}** (**3a**) and **$(C_{14}S)_6$PcCu-OPh-C_{60}** (**3b**), and the previous dyad, **$(C_{14}S)_6$PcCu-C_{12}-C_{60}** (**2c** in Fig. 2[A]) having a long *n*-alkylene spacer. When the Peak H height was normalized by the (1 0 0) reflection height for these dyads **3a**, **3b** and **2c**, we noticed interesting differences in these Peak H heights. The Peak H height of **2c** is nearly same as the (1 0 0) reflection height, whereas the Peak H heights of **3a** and **3b** are 1.5~2.5 times larger than those of the (1 0 0) reflections. This implies that the helical structures of fullerene moieties are formed in much longer distance for **3a** and **3b** than **2c**. Therefore, the fullerenes may more strongly aggregate for **3a** and **3b** than **2c**. Furthermore, the helical pitch values of Peak H are smaller for **3a** and **3b** (H = 61.3 Å and H = 58.7 Å) than that of **2c** (H = 71.5 Å). This means that the helical diameters are smaller for **3a** and **3b** than **2c**. Accordingly, the fullerenes are closer to the phthalocyanine cores for **3a** and **3b** than **2c**.

Fig. 7[B] shows X-ray diffraction patterns of the isotropic liquid (I.L.) at high temperatures for the present dyads, **3a** and **3b**, and the previous dyad **2c**. As can be seen from these X-ray diffraction patterns, Peak H appears even in these I.L.s. Very interestingly, the Peak H height in I.L. is larger than that of the (1 0 0) reflection for the present dyads, **3a** and **3b**, whereas the Peak H height is much smaller than that of the (1 0 0) reflection for the previous dyad **2c**. This implies that the aggregation of fullerenes is strongly kept in helical fashion even in the I.L.s of **3a** and **3b**, and weakly in the I.L. of the dyad **2c**, as schematically illustrated in this figure. To our best knowledge, it is the first example in I.L.s that such a strong helicity appears for **3a** and **3b**.

Homeotropic alignment depending on the presence of the methoxy group

As already mentioned above, homeotropic alignment could be observed for the dyad, **$(C_{14}S)_6$PcCu-VAN-C_{60}** (**3a**), having a methoxy group in the vanillin moiety, whereas it could not be observed for the **$(C_{14}S)_6$PcCu-OPh-C_{60}** (**3b**) dyad having no methoxy group at the phenoxy group. Hereupon, we wish to discuss about the homeotropic alignment depending on the presence of the methoxy group for these Pc-C_{60} dyads, **3a** and **3b**.

As can be seen from the large Peak H in Fig. 7[A], both of the dyads **3a** and **3b** showed strong helicity. Nevertheless, as can be seen from the photomicrographs in Fig. 5[A], homeotropic alignment could be observed for the dyad, **$(C_{14}S)_6$PcCu-VAN-C_{60}** (**3a**), having a methoxy group in the vanillin moiety, whereas it could not be observed for the **$(C_{14}S)_6$PcCu-OPh-C_{60}** (**3b**) dyad having no methoxy group at the phenoxy group. Therefore, presence of the methoxy group may be a key point on the homeotropic alignment. We have previously reported that a novel type of flying-seed-like liquid crystals show mesomorphism despite absence of long chains [36-41]. For example, **(*m*-CH_3OPhO)$_8$PcCu** (**8**) in Fig. 8[A] shows mesomorphism. The mesomorphism of flying-seed-like liquid crystals is originated from the free rotation or flip-flop of bulky substituents, *e.g.*, *m*-CH_3OPhO groups [39]. Therefore, the *o*-CH_3OPhO (**VAN**) group in **$(C_{14}S)_6$PcCu-VAN-C_{60}** (**3b**) may also enhance the mesomorphism and homeotropic alignment.

As shown in Fig. 8[B], the PhO group in **$(C_{14}S)_6$PcCu-OPh-C_{60}** (**3b**) can freely rotate together with fullerene moiety, so that coplanarity of the PhO group to the phthalocyanine core may collapse. Therefore, the first flat Pc core may incline to the glass surface and the Pc cores stack one after another to form columns inclined to the glass surface. Thus, the Col_{ho} mesophase of **3b** cannot achieve homeotropic alignment. On the other hand, the bulkier *o*-CH_3OPhO (**VAN**) group in **$(C_{14}S)_6$PcCu-VAN-C_{60}** (**3a**) may not freely rotate together with fullerene moieties among the nearest dyads, so that coplanarity of the PhO group to the phthalocyanine core may be maintained. Therefore, the first flat Pc core can flatly adhere to the glass surface and the Pc cores stack one after another to form columns perpendicular to the glass surface. Thus, the Col_{ho} mesophase of **3a** can achieve perfect homeotropic alignment.

It is very interesting that such a slight difference in these molecular structures between **3a** and **3b** becomes a crucial point to show the homeotropic alignment.

CONCLUSION

In this study, we have synthesized novel donor-acceptor dyads, **$(C_{14}S)_6$PcCu-VAN-C_{60}** (**3a**) and **$(C_{14}S)_6$PcCu-OPh-C_{60}** (**3b**), which are bridged between phthalocyanine (Pc) and fullerene (C_{60}) using or a natural product of vanillin or *p*-hydroxybenzaldehyde instead of the previous *n*-alkylene chain spacer, and established their mesomorphsim and homeotropic alignment between two glass plates.

Each of the dyads, **$(C_{14}S)_6$PcCu-VAN-C_{60}** (**3a**) and **$(C_{14}S)_6$PcCu-OPh-C_{60}** (**3b**), showed two Col_{ho} mesophases. Each of the Col_{ho} mesophases in **3a** and**3b** gave an additional very strong reflection named as Peak H in the very low angle region for their SAXS patterns. Peak H could be assigned to one pitch in a helical structure of the fullerenes around the Pc column. The Peak H height of the previous dyad **$(C_{14}S)_6$PcCu-C_{12}-C_{60}** (**2c**) is nearly same as the (1 0 0) reflection height, whereas the Peak H heights of **3a** and **3b** are 1.5~2.5 times larger than those of the (1 0 0) reflection. This implies that the helical structures of fullerene moieties are formed in much longer distance for **3a** and **3b** than **2c**.

Very interestingly, homeotropic alignment could be observed for the **$(C_{14}S)_6$PcCu-VAN-C_{60}** (**3a**) dyad having a methoxy group in the vanillin moiety, whereas it could not be observed for the **$(C_{14}S)_6$PcCu-OPh-C_{60}** (**3b**) dyad having no methoxy group at the phenoxy group. It is very noteworthy that such a slight difference in these molecular structures between **3a** and **3b** becomes a crucial point to show the homeotropic alignment.

REFERENCES

1. Li ZG, Zhao XY, Lu X, Gao ZQ, Mi BX, Huang W. *Science China-Chemistry*, 2012; **55**: 4, 553-578.
2. Zhao XY, Mi BX, Gao ZQ, Huang W. *Science China-Physics, Mechanics & Astronomy*, 2011; **54**: 3, 375-387.
3. Hiramoto M. *Journal of the Vacuum Society of Japan (Nippon Shinku Kyokai)*, 2010; **53**: 13-18.
4. Yoshikawa S. *Chemistry & Chemical Industry*, 2006; **59**: 960-963.
5. Bushby JR, Hamley IW, Liu Q, Lozman OR, Lydon EJ. *J Mater Chem.* 2005; **15**: 4429-4434.
6. Tashiro K, Aida T. *J Amer. Chem. Soc.* 2008; **130**: 13812-13813.
7. Thiebaut O, Bock H, Grelet E. *J. Am. Chem. Soc.* 2010; **132**: 6886-6887.
8. Bagui M, Dutta T, Chakraborty S, Melinger JS, Zhong H, Keightley A, Peng Z. *J. Phys. Chem. A* 2011; **115**: 1579-1592.
9. Haverkate LA, Zbiri M, Johnson MR, Deme B, de Groot HJM, Lefeber F, Kotlewski A, Picken SJ, Mulder FM, Kearley GJ. *J. Phys. Chem. B* 2012; **116**: 13098-13105.
10. Kato T, Ohta K. *The Proceedings of Annual Conference of Japanese Liquid Crystal Society*, 2006-09-15, 3B04 .
11. Uchida S, Kude Y, Nishikitani Y, Ota (= Ohta) K. *Jpn. Kokai Tokkyo Koho.* JP 2008214227(A)-2008-09-18 (Priority number: JP2007060604; Submission Date: 2007-03-09).
12. Shimizu M, Ohta K, Kato T. *The Proceedings of Annual Conference of Japanese Liquid Crystal Society*, 2008-09-17~19, 1c08.
13. de la Escosura A, Martınrez-Dıaz MV, Barbera J, Torres T. *J. Org. Chem.* 2008; **73**: 1475-1480.
14. Geerts YH, Debever O, Amato C, Sergeyev S. *Beilstein J. Org. Chem.* 2009; **5**: 1-9.
15. Tauchi L, Shimizu M, Ohta K. *The Proceedings of Annual Conference of Japanese Liquid Crystal Society*, 2009-09-13~15, 1C02.
16. Ota(= Ohta) K, *Jpn. Kokai Tokkyo Koho* ***(2011),*** JP2011132180(A)-2011-07-07 (Priority number: JP20090293501; Submission Date: 2009-12-24).
17. Nguyen-Tran HT, Tauchi L, Kamei T, Ohta K. *The Proceedings of the 90th CSJ Annual Meeting*, 2010-03-26~29, 3 E4-06.
18. Tauchi L, Shimizu M, Fujii T, Nguyen-Tran H-D, Kamei T, Ohta K. *The Proceedings of the 23rd International Liquid Crystal Conference*, 2010-07-11~16, Krakow Poland, P1.106.
19. Nihashi W, Hayashi H, Shimizu Y, Umeyama T, Matano Y, Imahori H. The Proceedings of The 39th Symmposium on The Fullerens, Nanotubes and Graphene Research Society, 2010-09-07, 3P-2.
20. Ohta K, Tauchi L, Nguyen-Tran HT, Shimizu M, Kamei T, Kato T. *The Proceedings of Pacifichem 2010*, Hawaii, USA, 2010-12-15~19, MATL-255, (Invited Lecture).
21. Tauchi L. Shimizu M, Ohta K, Itoh E. *The Proceedings of Pacifichem 2010*, Hawaii, USA, 2010-12-15~19, MATL-795.
22. Nguyen-Tran H-T, Tauchi L, Kamei T, Kato T, Ohta K, Itoh E. *The Proceedings of Pacifichem 2010*, Hawaii, USA, 2010-12-15~19, MATL-797.
23. Nakagaki T, Tauchi L, Shimizu M, Ohta K. *The Proceedings of the 91st CSJ Annual Meeting*, 2011-03-26~29, 3D3-55.
24. Nihashi W, Hayashi H, Umeyama T, Matano Y, Imahori H. *The Proceedings of the 91st CSJ Annual Meeting*, 2011-03-26~29, 2F2-13.
25. Hayashi H, Nihashi W, Umeyama T, Matano Y, Seki S, Shimizu Y, Imahori H. *J. Am. Chem. Soc.* 2011; **133**: 10736–10739. (Submission Date: 2011-04-26; Published 2011-06-23).

26. Ince M, Martinez-Diaz MV, Barbera J, Torres T. *J. Mater. Chem.* 2011; **21**: 1531-1536.
27. Kamei T, Kato T, Itoh E, Ohta K. *J. Porphyrins Phthalocyanines* 2012; **16**: 1261-1275.
28. Ariyoshi M, Sugibayashi-Kajita M, Suzuki-Ichihara A, Kato T, Kamei T, Itoh E, Ohta K. *J. Porphyrins Phthalocyanines* 2012; **16**: 1114-1123.
29. Shimizu M, Tauchi L, Nakagaki T, Ishikawa A, Itoh E, Ohta K. *J. Porphyrins Phthalocyanines* 2013; **17**: 264-282.
30. Tauchi L, Nakagaki T, Shimizu M, Itoh E, Yasutake M, Ohta K. *J. Porphyrins Phthalocyanines* 2013; **17**: 1080-1093.
31. Ishikawa A, Ono K, Ohta K, Yasutake M, Ichikawa M, and Itoh E. *J. Porphyrins Phthalocyanines* 2014; **18**: 366-379.
32. Watarai A, Yajima S, Ishikawa A, Ono K, Yasutake M and Ohta K, *ECS Transactions* 2015; **66**: 21-43.
33. Wöhrle D, Eskes M, Shigehara K and Yamada A, *Synthesis* 1993; 194-196.
34. Serin S, Karabörk M. *Synthesis and Reactivity in Inorganic and Metal-Organic Chemistry*, 2002; **32**: 9, 1635-1647.
35. Prato M, Maggini M and Scorrano G, *J. Am. Chem. Soc.* 1993; **115**: 9798-9799.
36. Ohta K, Shibuya T and Ando M, *J. Mater. Chem.* 2006; **16**: 3635-3639.
37. Takagi Y, Ohta K, Shimosuigi S, Fujii T and Itoh E, *J. Mater. Chem.* 2012; **22**: 14418–14425.
38. Hachisuga A, Yoshioka M, Ohta K and Itaya T, *J. Mater. Chem. C* 2013; **1**: 5315–5321.
39. Yoshioka M, Ohta K and Yasutake M, *RSC Advavces* 2015; **5**: 13828-13839.
40. Ishikawa A, Ohta K and Yasutake M, *J. Porphyrins Phthalocyanines* 2015; **19**: 639-650.
41. Watarai A, Ohta K and Yasutake M, *J. Porphyrins Phthalocyanines,* 2016; in press.

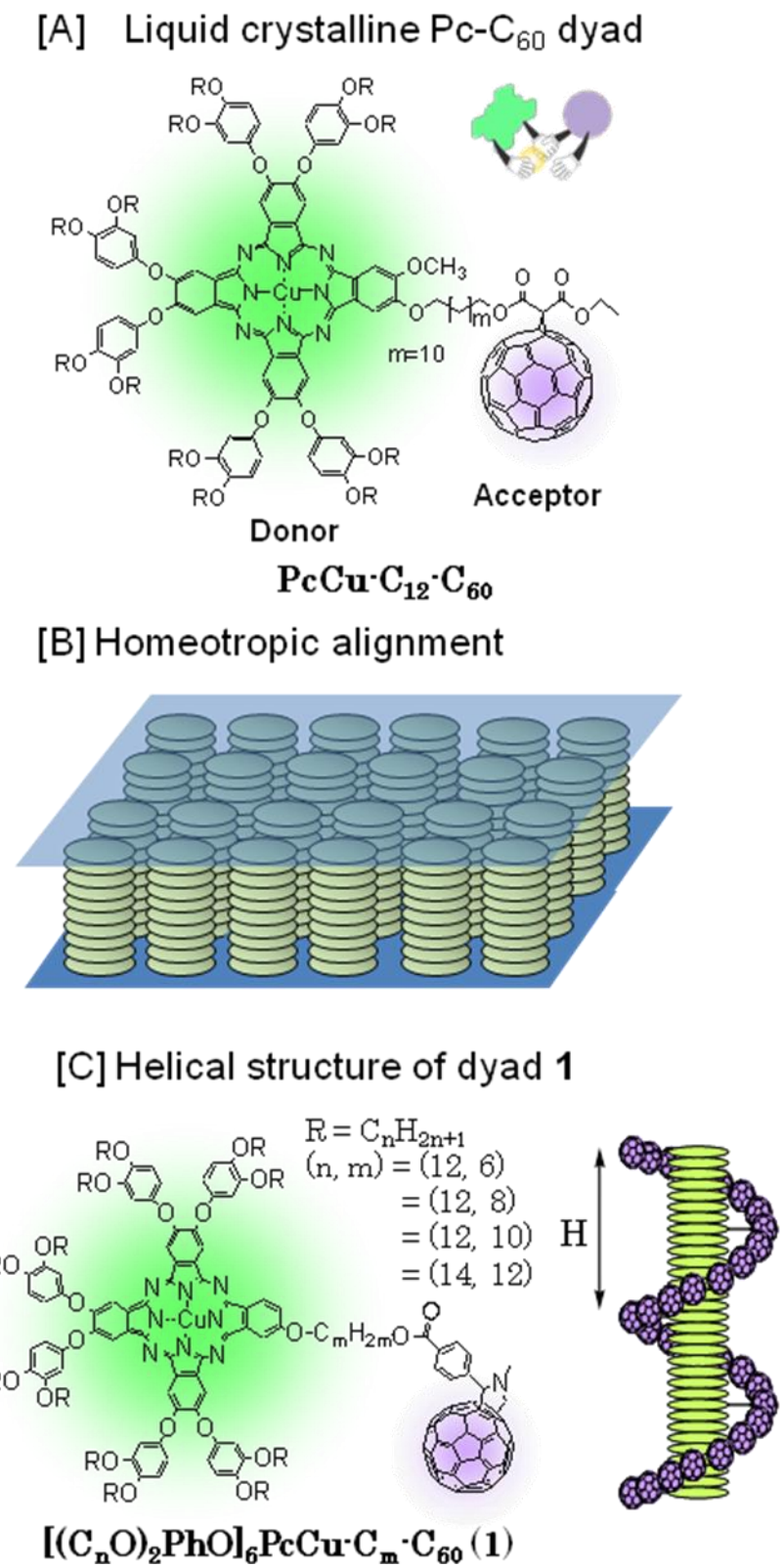

Fig. 1. Our developed phthalocyanine fullerene (Pc-C_{60}) dyads showing homeotropic alignment and helical structure.

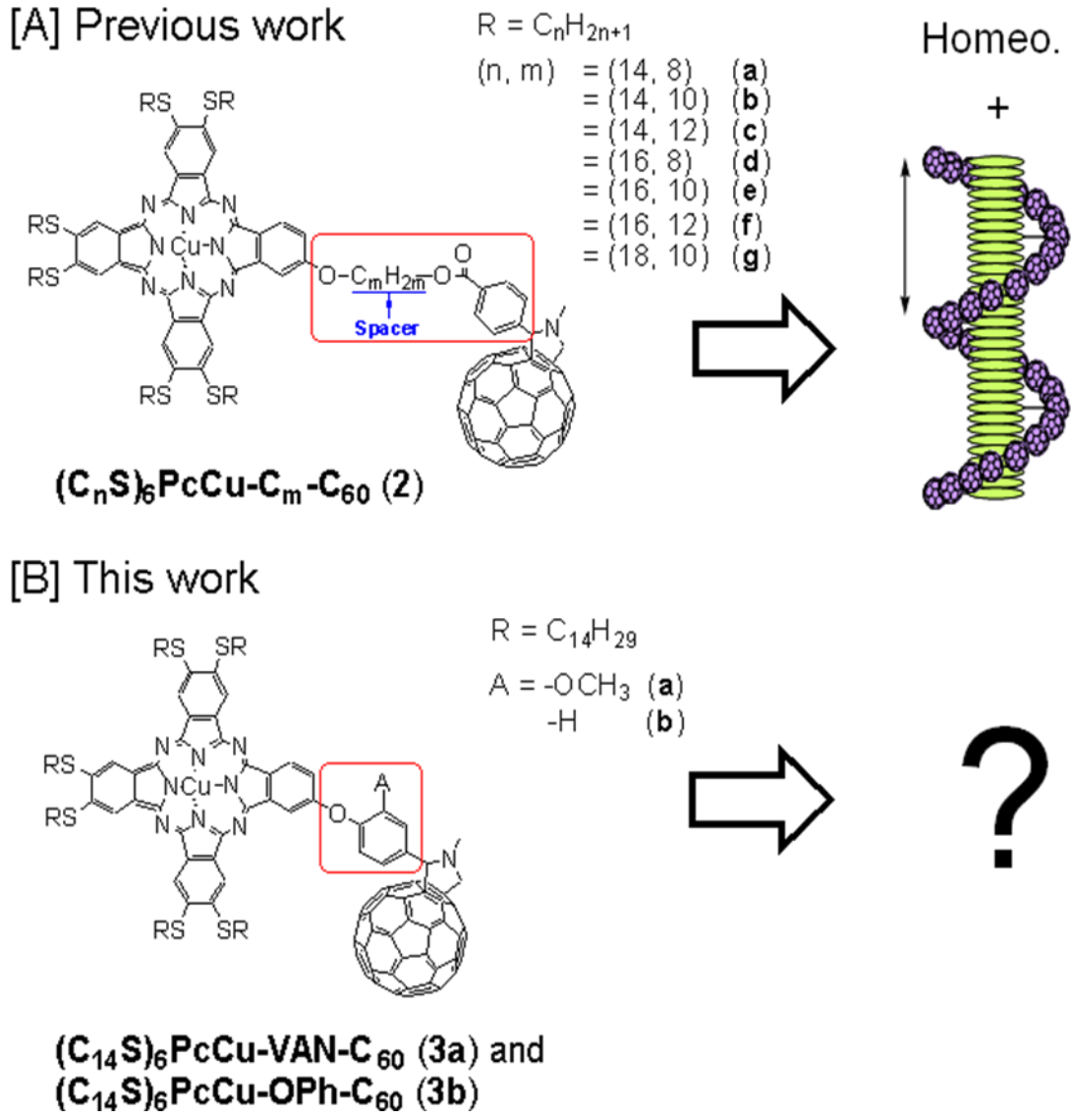

Fig. 2. Our previous and present works of the liquid crystals based on $(C_nS)_6PcCu\text{-}C_{60}$ dyad.

.

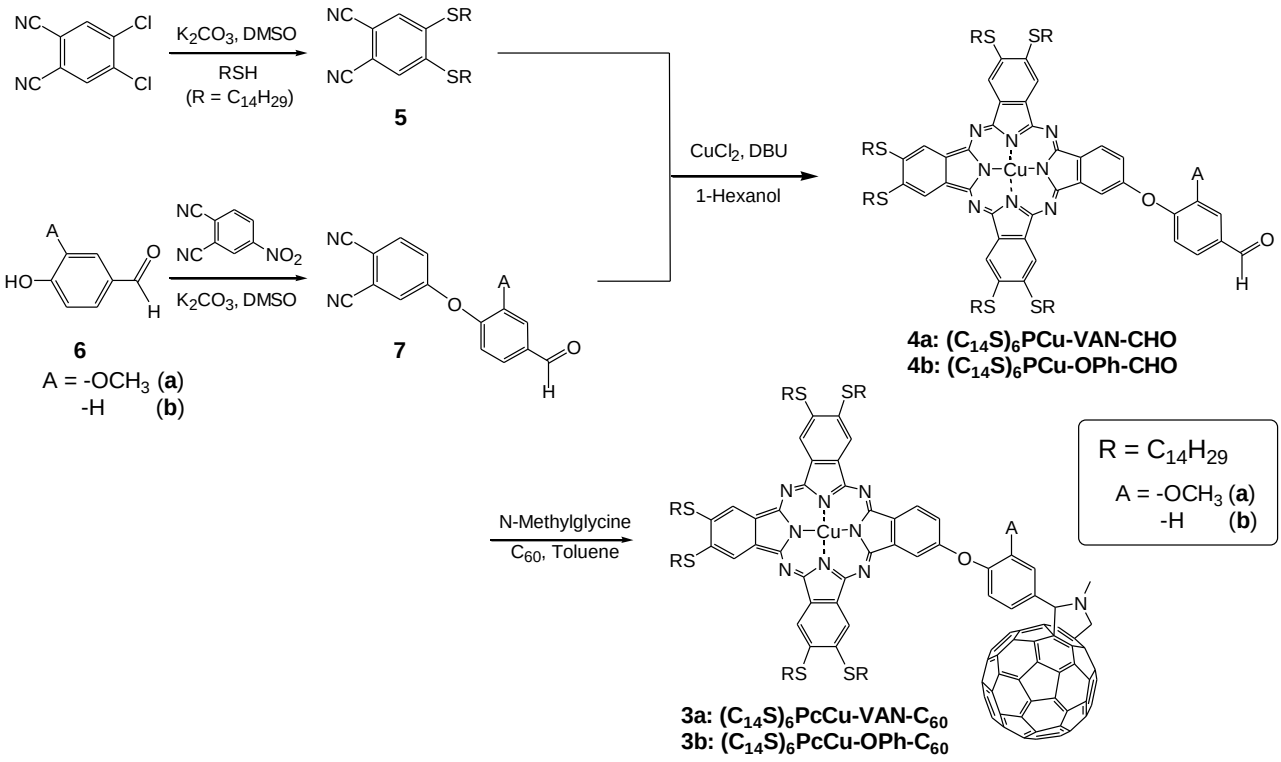

Scheme 1. Synthetic routes for **$(C_{14}S)_6$PcCu-VAN-C_{60}** (**3a**) and **$(C_{14}S)_6$PcCu-OPh-C_{60}** (**3b**).
DMSO = dimethylsulfoxide and DBU = 1,8-diazabicyclo[5,4,0]-undec-7-ene.

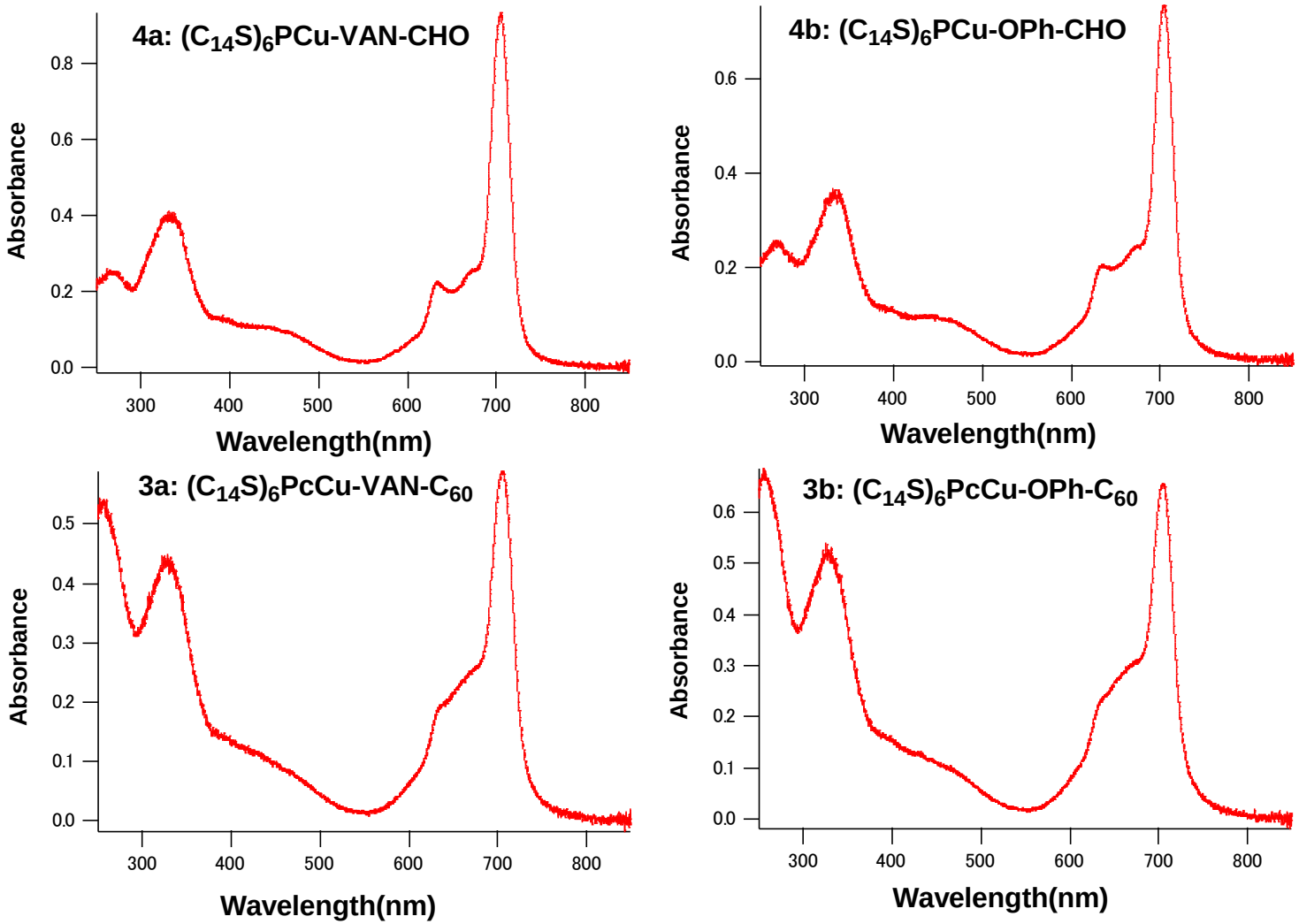

Fig. 3. UV-vis spectra of **4a-b** and **3a-b**. The spectral data are listed in Table S3.

Table 1. Phase transition temperatures and enthalpy changes of **4a-b** and **3a-b.**

Compound	Phase	$T/^{o}C$ [$\Delta H(kJmol^{-1})$]	Phase
4a: $(C_{14}S)_6$PcCu-VAN-CHO	Col_{ho}	298.1 [5.77] ⇌	I.L. (gr.dc.)
4b: $(C_{14}S)_6$PcCu-OPh-CHO	Col_{ho}	278.7 [2.84] ⇌	I.L. (gr. dc.)
3a: $(C_{14}S)_6$PcCu-VAN-C_{60}	$\boxed{Col_{ho1}}$	83.5 [1.37] ⇌ $\boxed{Col_{ho2}}$ 178.3 [0.89] ⇌	I.L.
3b: $(C_{14}S)_6$PcCu-OPh-C_{60}	Col_{ho1}	96.5 [1.93] ⇌ Col_{ho2} 176.7 [1.93] ⇌	I.L.

Phase nomenclature: Col_{ho} = hexagonal ordered columnar mesophase and I.L. = isotropic liquid.
$\boxed{\ }$ = mesophase showing homeotropic alignment. gr. dc. = gradual decomposition.

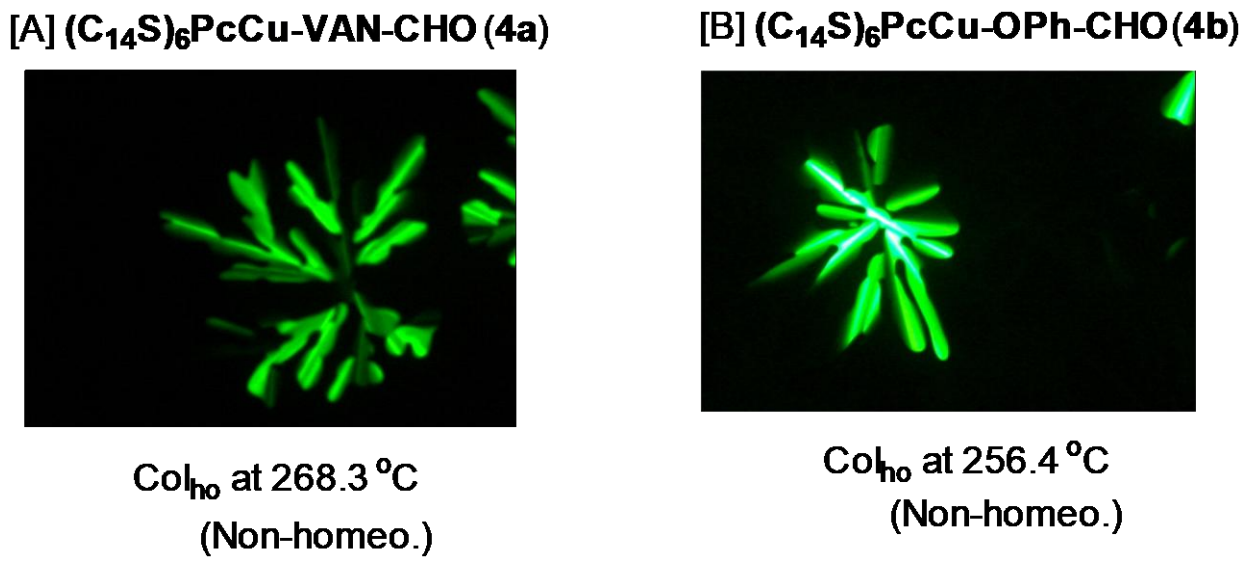

Fig. 4. Photomicrographs of the mesophases of **4a-b**.

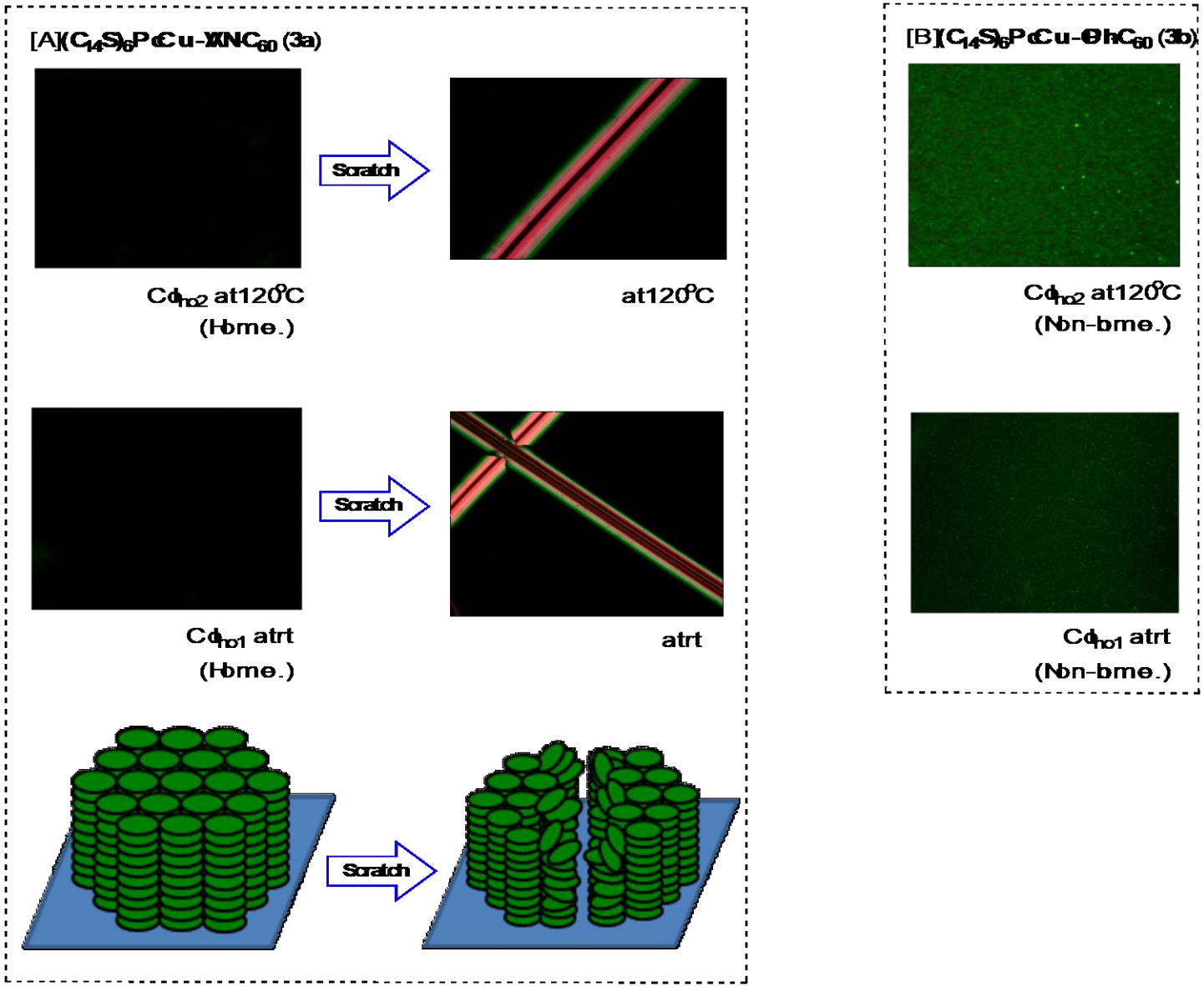

Fig. 5. Photomicrographs of the mesophases of **3a-b** at various temperatures and columnar alignment models.

Table 2. X-Ray data of compound **4a-b** and **1a-b**.

Compound (mesophase)	Lattice constants/Å	Spacing/Å		Miller indices
		Observed	Calculated	(*h k l*)
4a : $(C_{14}S)_6$PcCu-VAN-CHO		30.1	30.2	(1 0 0)
		17.2	17.4	(1 1 0)
(Col_{ho} at rt)	a = 34.8	11.1	11.3	(2 1 0)
	h = 3.38	8.24	8.36	(3 1 0)
	Z = 1.0 for ρ = 1.0	*ca.* 4.6	-	#
		3.38	-	(0 0 1)^h
4b : $(C_{14}S)_6$PcCu-OPh-CHO		31.9	31.9	(1 0 0)
		18.4	18.4	(1 1 0)
(Col_{ho} at rt)	a = 36.9	16.0	16.0	(2 0 0)
	h = 3.34	12.0	12.1	(2 1 0)
	Z = 1.0 for ρ = 0.90	*ca.* 4.6	-	#
		3.34	-	(0 0 1)^h
1a : $(C_{14}S)_6$PcCu-VAN-C_{60}		61.3	-	H
		31.3	31.3	(1 0 0)
(Col_{ho1} at rt)	a = 36.1	17.8	18.0	(1 1 0)
	h = 3.47	15.6	15.	(2 0 0)
	Z = 1.0 for ρ = 1.3	*ca.* 4.6	6 -	#
		3.47	-	(0 0 1)^h
		62.5	-	H
		31.5	31.4	(1 0 0)
(Col_{ho2} at 120 ^{o}C)	a = 36.2	18.1	18.1	(1 1 0)
	h = 3.52	15.5	15.7	(2 0 0)
	Z = 1.1 for ρ = 1.3	*ca.* 4.7	-	#
		3.52	-	(0 0 1)^h
		56.6	-	H
(I.L. at 250 ^{o}C)		30.7	-	(1 0 0)
		ca. 4.7	-	#
1b : $(C_{14}S)_6$PcCu-OPh-C_{60}		58.7	-	H
		29.6	29.6	(1 0 0)
(Col_{ho1} at r.t.)	a = 34.2	16.9	17.1	(1 1 0)
	h = 3.46	14.8	14.8	(2 0 0)
	Z = 0.97 for ρ = 1.3	*ca.* 4.5	-	#
		3.46	-	(0 0 1)^h
		59.9	-	H
		30.1	30.1	(1 0 0)
(Col_{ho2} at 120 ^{o}C)	a = 34.8	17.2	17.4	(1 1 0)
	h = 3.50	15.0	15.1	(2 0 0)
	Z = 1.0 for ρ = 1.3	*ca.* 4.7	-	#
		3.50	-	(0 0 1)^h
		58.2	-	H
(I.L. at 250 ^{o}C)		30.0	-	(1 0 0)
		ca. 4.5	-	#

= Halo of the molten alkyl chain. *h* = Stacking distance between the monomers. H = Helical pitch of the fullerenes. ρ : assumed density (g/cm^3).

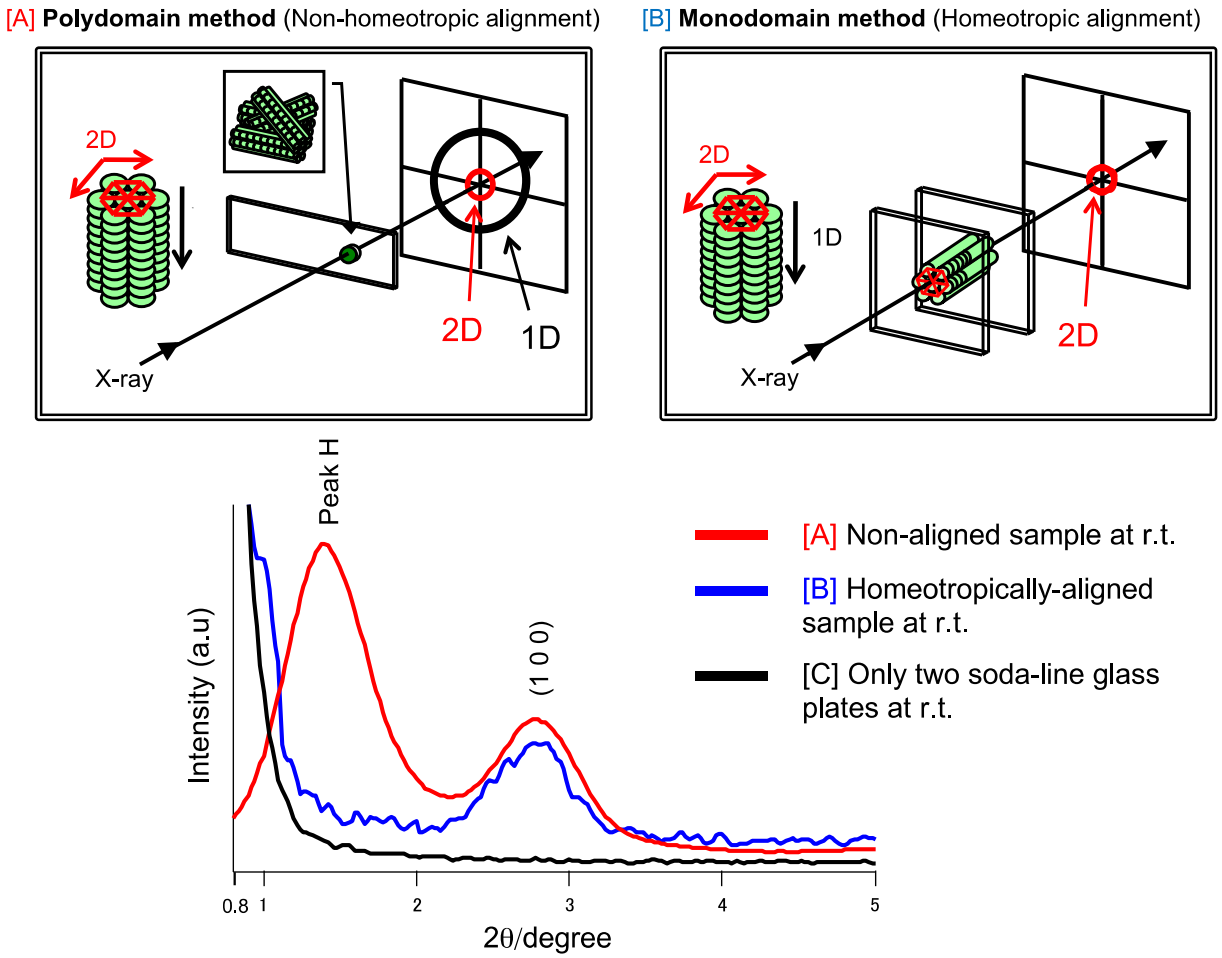

Fig. 6. Small angle X-ray diffraction patterns of **$(C_{14}S)_6$PcCu-VAN-C_{60} (3a)** for two different methods.

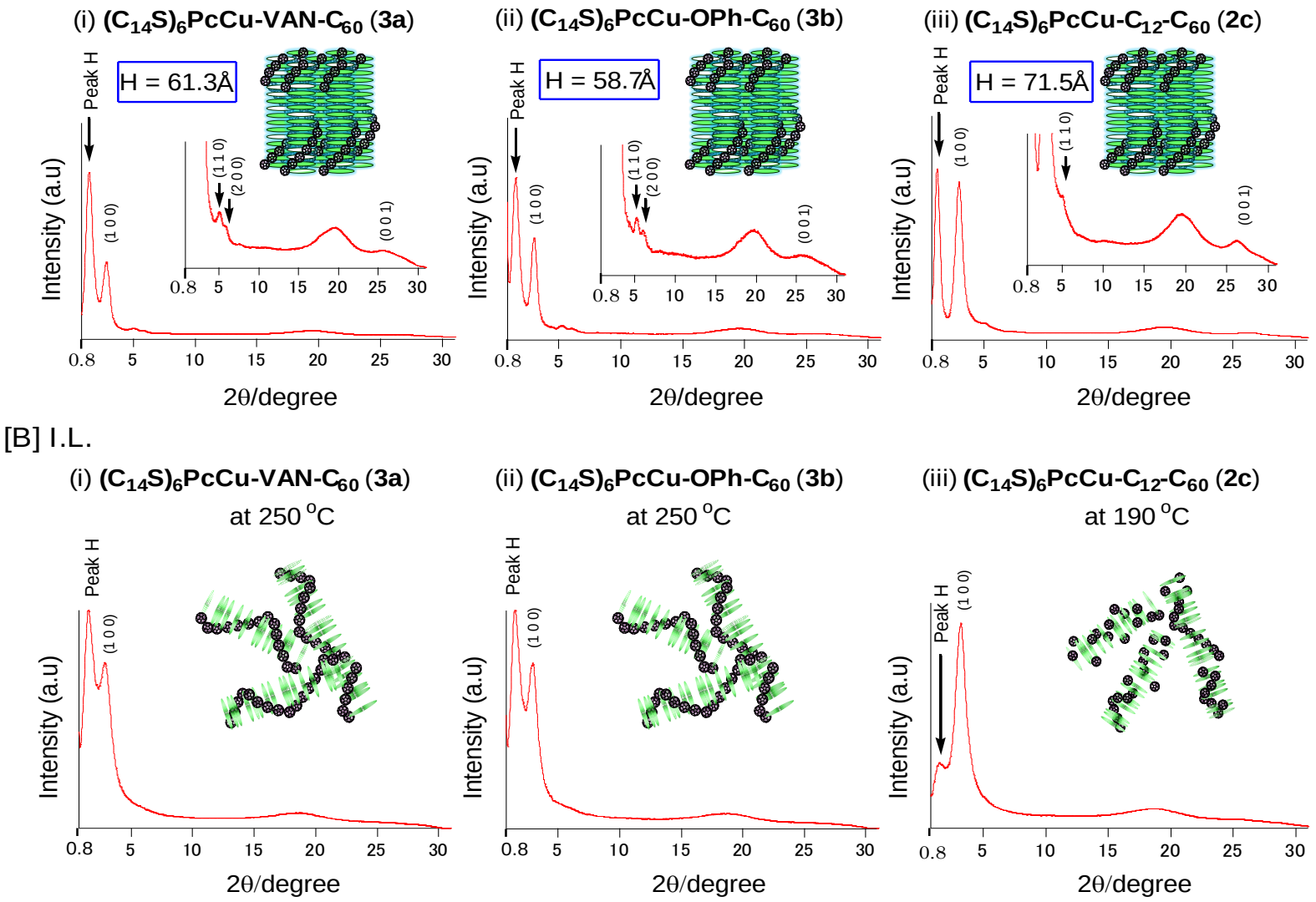

Fig. 7. Temperature-dependent small angle X-ray diffraction patterns of the Col$_{ho}$ mesophases and isotropic liquid of **3a**, **3b** and **2c**.

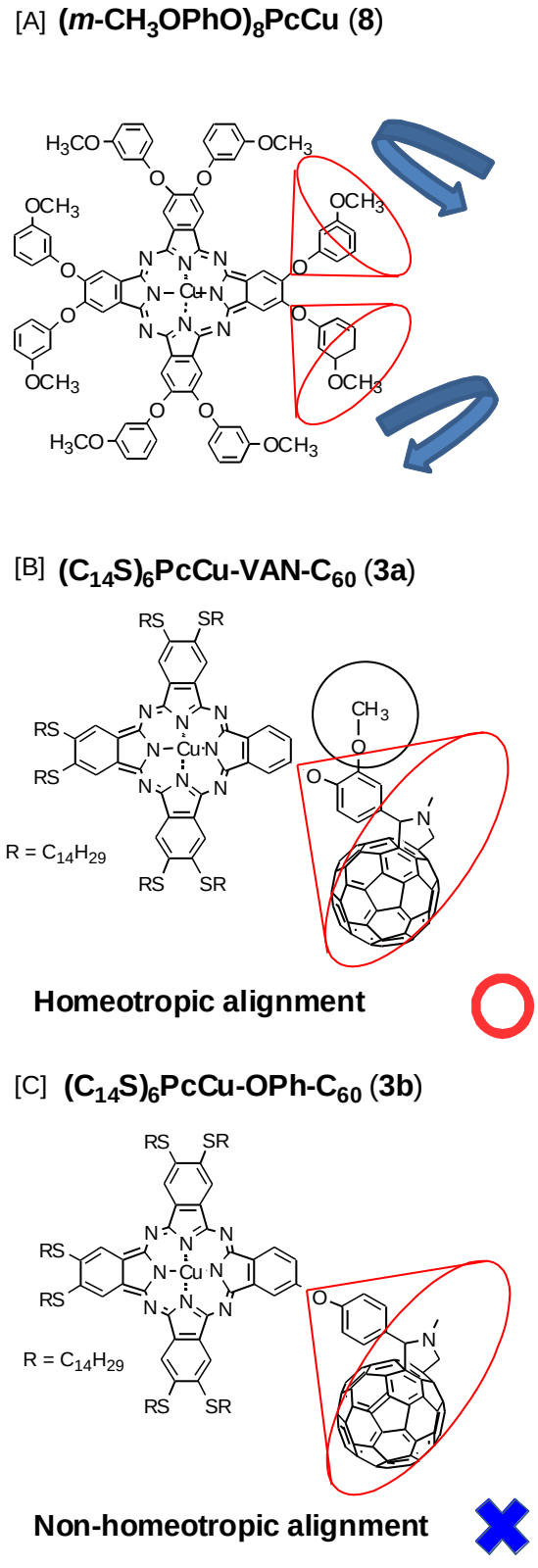

Fig. 8. Possible reason why the methoxy group induces the homeotropic alignment of **3a**. o = Restricted rotation of the bulky group by the additional methoxy group to induce homeotropic alignment. x = Free rotation may suppress to show homeotropic alignment.

SUPPLEMENTARY INFORMATION

Table S1. Elemental analysis data and yields of compound **4a-b** and **3a-b**.

Compound	Mol. formula (Mol. wt)	Elemental analysis: Found (Calcd.) (%)			Yield (%)
		C	H	N	
4a: $(C_{14}S)_6$PcCu-VAN-CHO	$C_{124}H_{190}N_8O_3S_6Cu$ (2096.84)	71.36 (71.03)	9.51 (9.13)	5.44 (5.34)	8.9
4b: $(C_{14}S)_6$PcCu-OPh-CHO	$C_{123}H_{188}N_8O_2S_6Cu$ (2066.82)	71.77 (71.48)	9.41 (9.17)	5.53 (5.42)	8.2
3a: $(C_{14}S)_6$PcCu-VAN-C_{60}*	$C_{186}H_{195}N_9O_2S_6Cu$ (2844.59)	—	—	—	28.6
3b: $(C_{14}S)_6$PcCu-OPh-C_{60}*	$C_{185}H_{193}N_9OS_6Cu$ (2814.57)	—	—	—	15.4

* This compound was too incombustible to carry out the elemental analysis.

Table S2. MALDI-TOF mass spectral data of compound **4a-b** and **3a-b**.

Compound	Exact mass formula (m/z = M+1)	Exact mass observed (m/z = M+1)
4a: $(C_{14}S)_6$PcCu-VAN-CHO	2094.26	2094.12
4b: $(C_{14}S)_6$PcCu-OPh-CHO	2064.25	2064.09
3a: $(C_{14}S)_6$PcCu-VAN-C_{60}	2842.57	2842.32, 2121.36*
3b: $(C_{14}S)_6$PcCu-OPh-C_{60}	2811.81	2812.19, 2091.31*

* = M^+ - 720

Table S3. UV-vis spectral data of compound **4a-b** and **3a-b**.

Compound	Concentration[#] ($X10^{-5}$mol/l)	λ_{max} (nm) (logε)						
		C_{60} peak	Soret-band			Q-band		
						Q_{0-1} band	*	Q_{0-0} band
4a: $(C_{14}S)_6$PcCu-VAN-CHO	0.500	-	266.9 (4.70)	330.6 (4.91)	*ca.* 463 (4.27)	634.0 (4.66)	669.3 (4.70)	705.0 (5.27)
4b: $(C_{14}S)_6$PcCu-OPh-CHO	0.499	-	269.0 (4.71)	334.7 (4.86)	*ca.* 462 (4.26)	635.6 (4.61)	674.4 (4.69)	703.7 (5.18)
3a: $(C_{14}S)_6$PcCu-VAN-C_{60}	0.498	256.8 (5.04)	-	328.9 (4.95)	*ca.* 470 (4.19)	*ca.* 631 (4.57)	*ca.* 664 (4.69)^0	703.8 (5.07)
3b: $(C_{14}S)_6$PcCu-OPh-C_{60}	0.501	257.7 (5.13)	-	331.1 (5.02)	*ca.* 478 (4.23)	*ca.* 633 (4.66)	*ca.* 668 (4.78)^0	704.0 (5.12)

#: In chloroform. *: Aggregation band of Q_{0-0} band. ^{0}: Shoulder.

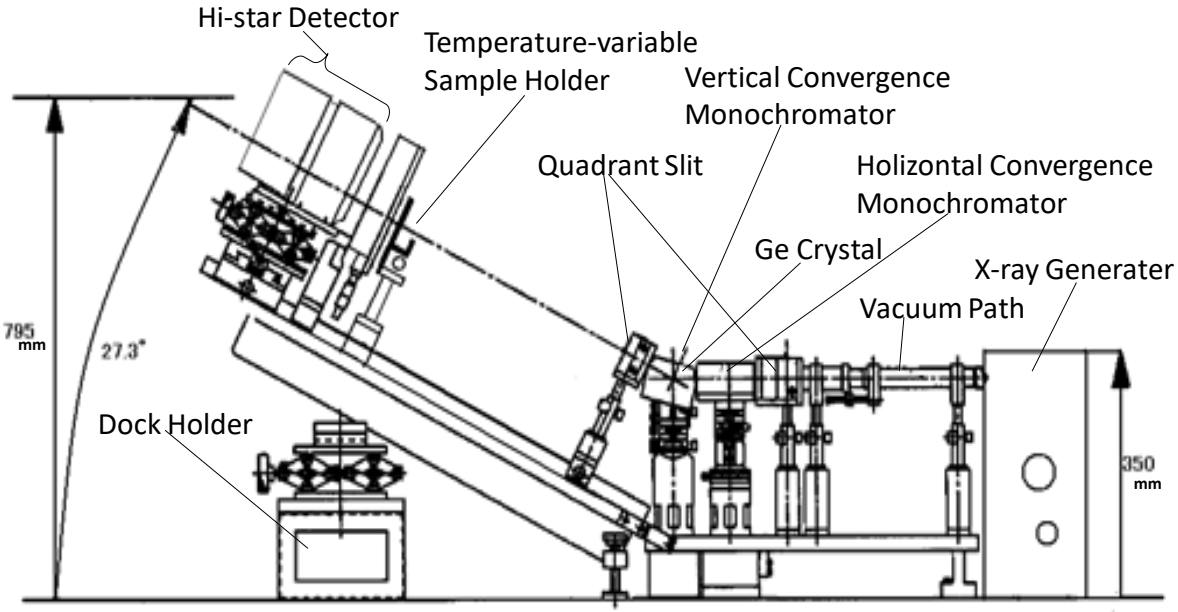

Fig. S1. Setup of Small-Angle X-ray Scattering (Bruker MAC SAXS) equipped with a temperature-variable sample holder.

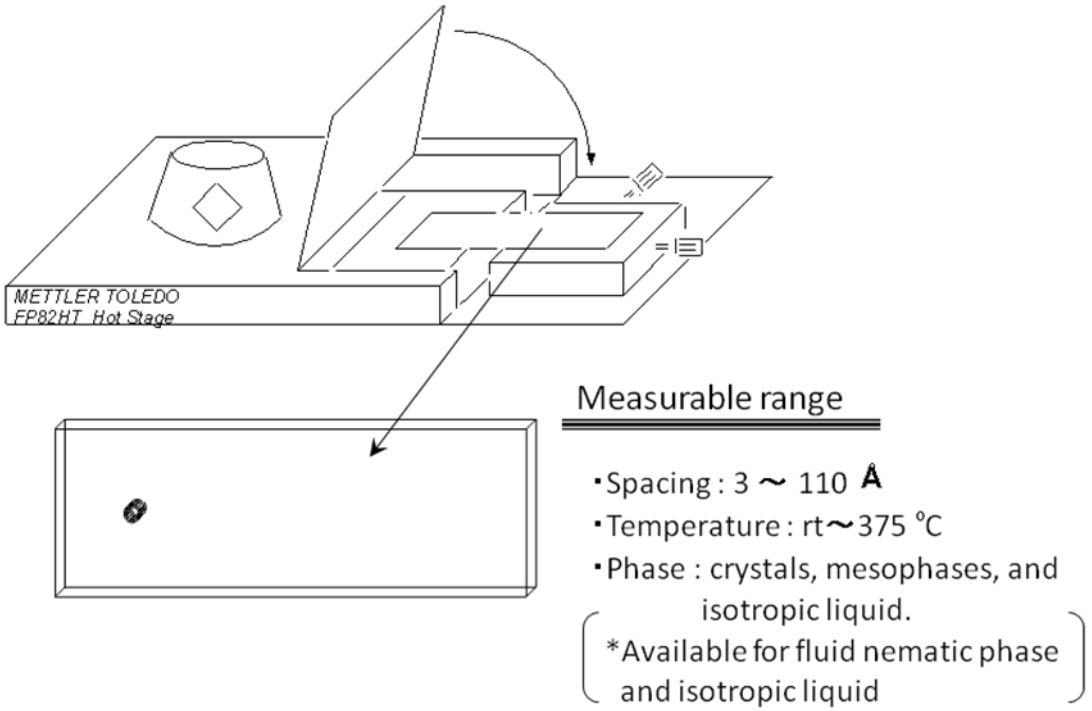

Fig. S2. Setup of the temperature-variable sample holder.